

Zak phase reconstruction enabled by thermal motion of atoms

Ruosong Mao^{1,*}, Xingqi Xu^{1,*}, Jiefei Wang^{1,*}, Chenran Xu¹,
Gewei Qian¹, Han Cai^{1,†}, Shi-Yao Zhu¹, and Da-Wei Wang^{1,2}

¹*Interdisciplinary Center for Quantum Information,
State Key Laboratory of Modern Optical Instrumentation,
and Zhejiang Province Key Laboratory of Quantum Technology and Device,
Department of Physics, Zhejiang University, Hangzhou 310027, Zhejiang Province, China and*
²*CAS Center for Excellence in Topological Quantum Computation,
University of Chinese Academy of Sciences, Beijing 100190, China*

(Dated: November 25, 2021)

Ultracold atoms provide a flexible platform for simulating topological phases. However, they are intrinsically prone to thermal noise, which can overwhelm topological response and hamper promised applications. On the other hand, topological invariants can be reconstructed from the energy spectra of particles subjected to a static force, based on the polarization relation between Wannier-Stark ladders and Zak phases. Such spectroscopic methods circumvent the obstacle to measuring topological invariants in thermal atoms. Here we reconstruct Zak phases from the anti-crossing between Wannier-Stark ladders in room-temperature superradiance lattices. Without dynamical manipulation routinely needed in ultracold atoms, we evaluate Zak phases directly from the absorption spectra. The thermal atomic motion, an essential source of noise in cold atoms, plays a key role in extracting Zak phases. Our approach paves the way of measuring topological invariants and developing their applications in room-temperature atoms.

Topological matter has promising applications in noise resilient devices and quantum information processing [1, 2], thanks to the robust topological response guaranteed by global geometric quantities of the Bloch bands, namely, the topological invariants [3–6]. These invariants only change stepwisely when the bulk goes through a topological phase transition, which involves band gap closing and reopening. Characterizing topological invariants is a central task in synthesizing and simulating topological phases. They are usually measured by the response from gapless edge states based on the bulk-edge correspondence. However, edges are not always available in atomic quantum simulators [7, 8]. New methods in measuring topological invariants in bulk are highly wanted. Along this line techniques based on reciprocal-space interference [9, 10], quench dynamics [11, 12], and Hall transport [13, 14] have been developed in atomic simulators.

Previous experiments of determining topological invariants from bulk response in ultracold atoms rely on dynamic evolution or adiabatic manipulation [9–14]. On the other hand, spectroscopic methods [15–19] have been proposed to measure the topological invariants by applying a constant force which turns the Bloch energy bands into Wannier-Stark ladders (WSLs) [20] with equidistant discrete energies. In one-dimensional (1D) systems, the energies of the WSLs are determined by Wannier centers (WCs) [21] reflecting the Zak phases [3] of the energy bands [22–24]. Such spectroscopic methods circumvent the requirements of atom cooling and enable the measurement of topological invariants in thermal atoms.

Here we report the reconstruction of Zak phases of the Rice-Mele (RM) model [25] through the anti-crossing between the WSLs of superradiance lattices [26–28], which

are momentum-space lattices of timed Dicke states [29]. The Doppler shift of moving atoms introduces an effective force in the superradiance lattice. Different velocity groups of thermal atoms provide a set of continuous values of the effective force, which results in WSLs with energies determined by the Zak phases [15, 17]. The absorption spectra of superradiance lattices are characterized by peaks and dips due to the anti-crossing between the WSLs from different energy bands. We obtain the Zak phases from the locations of the anti-crossing points. Two celebrated versions of the RM model, the Semenoff insulator and the Su-Shrieffer-Heeger (SSH) model [30], are investigated in detail. We also demonstrate the Zak phase reconstruction for general RM models. Our approach can be generalized to identify topological invariants in higher dimensions [31–35].

We perform the experiment with the hyperfine levels of the ^{87}Rb D1 line in a standing-wave-coupled EIT configuration, as shown in Fig. 1(a) (see the complete setup in Supplemental Material [36]). A weak probe field propagating in x direction couples the ground state $|g\rangle \equiv |5^2S_{1/2}, F=1\rangle$ to the excited state $|b\rangle \equiv |5^2P_{1/2}, F=2\rangle$. The excited state is also coupled to a metastable state $|a\rangle \equiv |5^2S_{1/2}, F=2\rangle$ by two strong counter-propagating light fields, forming a 1D bipartite superradiance lattice [26, 27]. The absorption spectra of the probe field is used to obtain the Zak phases of the superradiance lattices.

In order to clarify the effect of atomic motion, we start by analysing the contribution from atoms with different velocities in x direction. For atoms in each velocity group, the opposite Doppler shifts of the two coupling fields lead to a linear potential in momentum-space [26, 40] (we set $\hbar = 1$ and see details in Supplemental

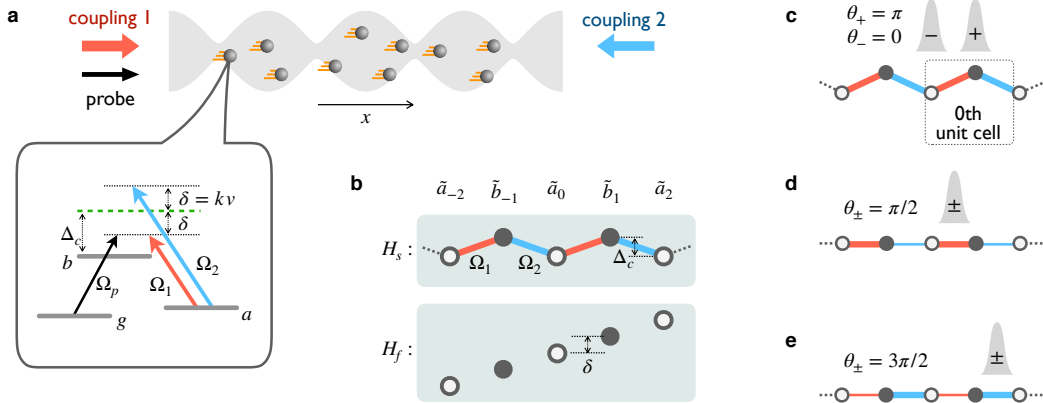


Figure 1. **Rice-Mele superradiance lattices of moving atoms.** (a) Schematic configuration of the light fields and the coupling between the Doppler shifted light fields and the atomic levels in the reference frame of the atom (inset). The shaded area indicates the envelope of the standing wave coupling field and the balls indicate atoms with velocity v . (b) The superradiance lattice Hamiltonian H_s and the linear potential Hamiltonian H_f . (c) The Semenoff insulator with $\Omega_1 = \Omega_2$, $\Delta_c \neq 0$. The shaded areas indicate the positions of the Wannier functions in a unit cell for upper (+) and lower (-) bands. Two distinct topological phases of the SSH model are depicted in (d) $\Delta_c = 0$, $\Omega_1 > \Omega_2$ and (e) $\Delta_c = 0$, $\Omega_1 < \Omega_2$.

Material [36]),

$$H_f = \delta \sum_j [2j\hat{a}_{2j}^\dagger \hat{a}_{2j} + (2j+1)\hat{b}_{2j+1}^\dagger \hat{b}_{2j+1}], \quad (1)$$

where the Doppler shift $\delta \approx k_c v \approx k_p v$ with k_p (k_c) being the probe (coupling) field wave vector amplitude and v being the velocity of the atoms in x direction, $\hat{d}_j^\dagger = \sqrt{1/N} \sum_m |d_m\rangle \langle g_m| \exp(ik_j x_m)$ ($d = a, b$) is the creation operator of the timed-Dicke state [29] $|\tilde{d}_j\rangle \equiv \hat{d}_j^\dagger |g_1, g_2, \dots, g_N\rangle$ with wave vector $k_j = k_p + (j-1)k_c \approx jk_c$ (j is an integer), m labels the m th atom at the position x_m , N is the total number of atoms within the velocity range $[v - \Gamma/2k_c, v + \Gamma/2k_c]$ where v satisfies the Maxwell distribution and Γ is the decay rate of the state $|b\rangle$.

The total Hamiltonian $H = H_s + H_p + H_f$, where H_s and H_p are interaction Hamiltonians involving the coupling and probe fields, respectively. H_s is the tight-binding Hamiltonian of the RM superradiance lattices [26–28], as shown in Fig. 1(b),

$$H_s = \sum_j \Delta_c \hat{a}_{2j}^\dagger \hat{a}_{2j} + [\hat{a}_{2j}^\dagger (\Omega_1 \hat{b}_{2j+1} + \Omega_2 \hat{b}_{2j-1}) + \text{H.c.}], \quad (2)$$

where Ω_1 and Ω_2 are the Rabi frequencies of the co-propagating and counter-propagating coupling fields, and $\Delta_c = \nu_c - \omega_{ba}$ with ν_c being the coupling field frequency and ω_{ba} being the transition frequency between states $|a\rangle$ and $|b\rangle$. The timed Dicke state $|\tilde{b}_1\rangle$ in the superradiance lattice can be created from the ground state by $H_p = \sqrt{N} \Omega_p e^{-i\Delta_p t} \hat{b}_1^\dagger + \text{H.c.}$, where the probe detuning $\Delta_p = \nu_p - \omega_{bg}$ with ν_p being the probe field frequency and ω_{bg} being the transition frequency between states $|b\rangle$ and $|g\rangle$.

The WCs are the expectation positions of the Wannier functions [24]. For the Hamiltonian H_s , the WCs in the n th unit cell $r_\pm^{[n]}$ for the upper (+) and lower (-) bands are related to the geometric Zak phases by (in unit of distance between neighboring lattice sites) [22, 23],

$$r_\pm^{[n]} = 2n + \theta_\pm/\pi, \quad (3)$$

where the Zak phases $\theta_\pm \equiv i \int dx \langle u_\pm(x) | \partial_x | u_\pm(x) \rangle$ with $|u_\pm(x)\rangle$ being the periodic Bloch functions in real space and the integration is over the whole Brillouin zone. Therefore, the Zak phases are the fractional parts of the corresponding WCs [22, 23], as schematically depicted in Fig. 1(c)–(e). The values of the Zak phases are gauge dependent due to the freedom in choosing the origin of the unit cell [9]. Throughout this work, the gauge is uniquely fixed by the zero energy point of H_f (see Fig. 1(c)).

In the presence of a weak static force described by the Hamiltonian H_f , the energy spectra split into discrete WSLs [15, 17, 40, 41],

$$E_\pm^{[n]}(\delta) = \varepsilon_\pm + r_\pm^{[n]} \delta, \quad (4)$$

where ε_\pm denote the energies of the Bloch band centers (bc), defined as the average band energies of H_s . From Eqs. (3) and (4), the Zak phases are obtained by $\theta_\pm = (\partial E_\pm^{[n]}/\partial \delta - 2n)\pi$.

The relation in Eq. (4) can be seen from the absorption spectra in Fig. 2(a)–(c) as functions of δ for three different RM lattices, namely, the Semenoff insulator with $\theta_- = \pi$, $\theta_+ = 0$ (Fig. 2(a)), and two topologically distinct phases of SSH model with half-integer Zak phases $\theta_\pm = 0.5\pi$ (Fig. 2(b)) and $\theta_\pm = 1.5\pi$ (Fig. 2(c)). In the weak force regime where the coupling between the WSLs from different bands are negligible, the spectra

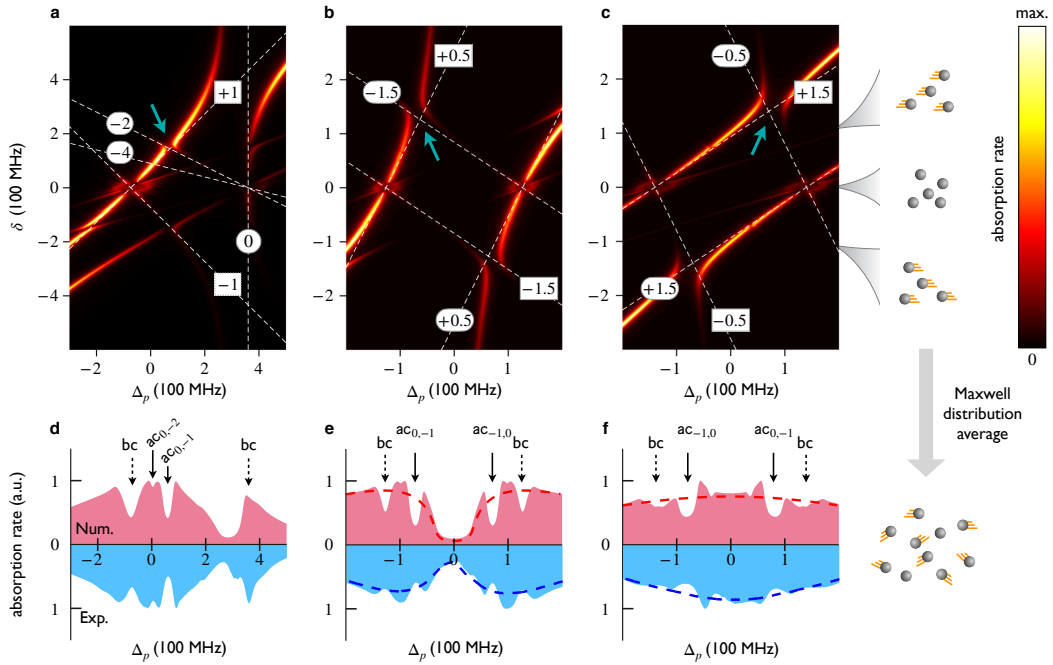


Figure 2. Wannier-Stark ladders and the absorption spectra of the superradiance lattices. (a)-(c) The absorption spectra as functions of the Doppler shift δ and probe detuning Δ_p . The white dashed lines indicate the uncoupled WSLs in Eq. (4). The highlighted numbers denote the values of $r_-^{[n]}$ (square) and $r_+^{[n]}$ (round) of the corresponding WSLs. The cyan arrows mark the anti-crossing $ac_{0,-1}$. (a) and (d) $\Omega_1 = \Omega_2 = 120$ MHz and $\Delta_c = 298$ MHz; (b) and (e) $\Omega_1 = 125$ MHz, $\Omega_1/\Omega_2 = 5.3$, and $\Delta_c = 0$; (c) and (f) $\Omega_2 = 138$ MHz, $\Omega_1/\Omega_2 = 0.17$, and $\Delta_c = 0$. (d)-(f) The absorption spectra of the room-temperature superradiance lattices. The experimental data and numerical simulation (obtained by integrating δ in (a)-(c)) are shaded with blue and red colors, respectively. The dips and peaks in the spectra capture the locations of the band centers (bc) and anti-crossing points (ac_{n,m}). The blue and red dashed lines show the dimerized limits of (e) $\Omega_2 = 0$ and (f) $\Omega_1 = 0$. It is schematically shown that a δ corresponds to atoms with a certain velocity and the absorption spectra are obtained by integrating δ .

follow the linear dependence in Eq. (4) as indicated by the dashed lines. The brightest ladders in the absorption spectra are the ones corresponding to $r_{\pm}^{[0]} = \theta_{\pm}/\pi$ in the 0th unit cell, which contains the state $|\tilde{b}_1\rangle$. The absorption rate is proportional to the projected density of states (PDOS) on the state $|\tilde{b}_1\rangle$, i.e., $\sum_l \delta_D(\Delta_p - E_l) |\langle \psi_l | \tilde{b}_1 \rangle|^2$, where $\delta_D(\Delta_p - E_l)$ is the Dirac delta function, $|\psi_l\rangle$ and E_l are the eigenstates and eigenenergies satisfying $(H_s + H_f)|\psi_l\rangle = E_l|\psi_l\rangle$ [36].

When a pair of WSLs from different bands ($E_+^{[n]}$ and $E_-^{[m]}$) have the same energy for a large δ , the inter-band coupling removes their degeneracy and results in an anti-crossing [41, 42] denoted by $ac_{n,m}$. Their positions in the energy-force diagram can be estimated by the degeneracy points of the uncoupled WSLs [43] satisfying $E_-^{[n]}(\delta) = E_+^{[m]}(\delta) = \Delta_{n,m}$, where $\Delta_{n,m}$ is the probe detuning of the corresponding anti-crossing point. The anti-crossing $ac_{0,-1}$, marked by the arrow in Fig. 2(a), is due to the coupling between the WSLs $E_-^{[0]} = \varepsilon_- + \delta$ and $E_+^{[-1]} = \varepsilon_+ - 2\delta$, from which we obtain $\delta = (\varepsilon_+ - \varepsilon_-)/3$ and $\Delta_{0,-1} = (\varepsilon_+ + 2\varepsilon_-)/3$. On the other hand, for the half-integer topological invariants of

the SSH models, the prominent anti-crossing $ac_{0,-1}$ locates at $\delta = (\varepsilon_+ - \varepsilon_-)/2$ and $\Delta_{0,-1} = (\varepsilon_+ + 3\varepsilon_-)/4$ in Fig. 2(b) and $\Delta_{0,-1} = (3\varepsilon_+ + \varepsilon_-)/4$ in Fig. 2(c). The values of $\Delta_{n,m}$ obtained from the absorption spectra are the key to extract the Zak phases.

The absorption of the superradiance lattice is contributed by all atoms with velocities in Maxwell distribution [44]. We obtain Fig. 2(d)-(f) from the WSLs in Fig. 2(a)-(c) by integrating δ , which has a distribution width about 500 MHz and covers all relevant values for the Zak phase reconstruction. The anti-crossings and band centers modify the PDOS drastically and their signatures can be easily picked out in the absorption spectra, as shown in Fig. 2(d)-(f). In particular, we notice that the anti-crossing leads to the decrease of PDOS, yielding a dip in the absorption spectra. The band centers are characterized by a dip in most cases or a peak (for the upper band center when $\Delta > 0$), due to the modification of the PDOS of the state $|\tilde{b}_1\rangle$ resulted from Wannier-Stark localization [45].

In order to reconstruct the Zak phases, we shall quantify the common features in the absorption spectra of lattices with the same Zak phase. In Fig. 3(a), we main-

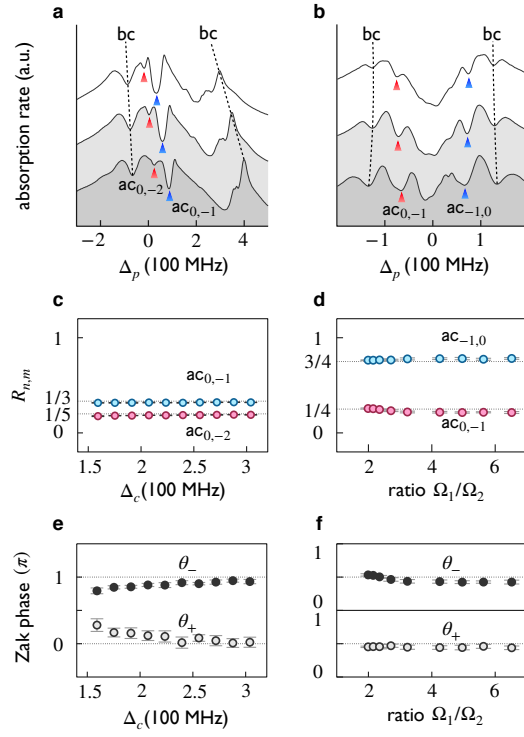


Figure 3. Zak phase reconstruction from the absorption spectra of the superradiance lattices. The experimental absorption spectra for (a) the Semenoff insulator superradiance lattices with $\Omega_{1,2} = 120$ MHz and $\Delta_c = 174, 232$, and 298 MHz from top to bottom, and (b) the SSH superradiance lattices with $\Delta_c = 0$, $\Omega_1 = 118$ MHz, and $\Omega_1/\Omega_2 = 6.52, 4.25$, and 2.15 from top to bottom. We use the marked extrema in absorption peaks and dips to locate the band centers and anti-crossings. (c) The measured $R_{n,m}$ (points) compared with the normalized ratio of WCs (dashed lines) for (d) the Semenoff insulator and (e) the SSH superradiance lattices, from which we reconstruct the Zak phases θ_{\pm} in (e) and (f). Error bars are obtained from four independent data sets (see Supplemental Material [36] for WSLs and more absorption spectra).

tain $\Omega_1 = \Omega_2 = 120$ MHz and decrease Δ_c from bottom to top. The Zak phase is the same but the coupling between WSLs increases to widen the anti-crossing gap. We locate the absorption dips due to the anti-crossing points with its normalized energy,

$$R_{n,m} = (\Delta_{n,m} - \epsilon_-)/(\epsilon_+ - \epsilon_-), \quad (5)$$

where $\Delta_{n,m}$ are measured from the absorption dip minima due to $ac_{n,m}$. On the other hand, according to the geometry of WSLs in the Δ_p - δ diagram, $R_{n,m}$ is approximately the normalized ratio of WCs between the WSLs,

$$R_{n,m} \approx \frac{r_-^{[n]}}{r_-^{[n]} - r_+^{[m]}} = \frac{2n\pi + \theta_-}{(2n\pi + \theta_-) - (2m\pi + \theta_+)}. \quad (6)$$

In Fig. 3(c), we obtain $R_{0,-2} \approx 1/5$, $R_{0,-1} \approx 1/3$. We solve two equations of θ_{\pm} from the values of $R_{0,-1}$ and

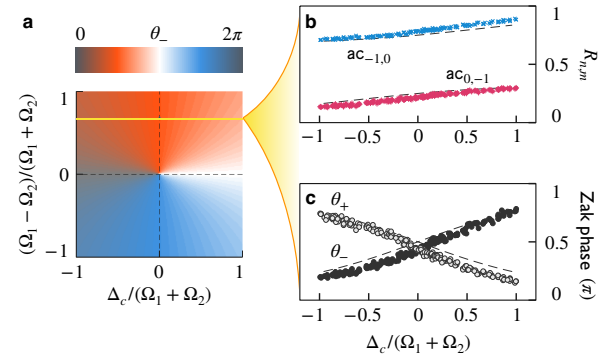


Figure 4. Zak phase reconstruction of Rice-Mele superradiance lattices. (a) The Zak phase diagram of the RM model as a function of Δ_c and $\Omega_1 - \Omega_2$. (b) Locations of the anti-crossing points and (c) values of the Zak phases are measured along the yellow line in (a) with $\Omega_1 = 125$ MHz and $\Omega_1/\Omega_2 = 5.3$, compared with their theoretical values (dashed lines). The plots contain 200 data sets (see Supplemental Material [36] for WSLs and absorption spectra).

$R_{0,-2}$ and conclude that $\theta_- \approx \pi$ and $\theta_+ \approx 0$, as shown in Fig. 3(e).

For the SSH models, we keep $\Delta_c = 0$ and tune the Rabi frequencies of the two coupling fields from almost dimerization to the topological phase transition point. The Zak phases are maintained the same while the anti-crossing energy gaps increase from top to bottom in Fig. 3(b). The measured $R_{n,m}$ in Fig. 3(d) agree well with their expected values and the reconstructed Zak phases are obtained, $\theta_{\pm} \approx 0.5\pi$, as shown in Fig. 3(f).

For a general RM Hamiltonian, i.e., H_s with $\Omega_1 \neq \Omega_2$ and $\Delta_c \neq 0$, the Zak phases are neither integers nor half-integers. Along the yellow line in the phase diagram in Fig. 4(a), we measure the absorption spectra to obtain $R_{0,-1}$ and $R_{-1,0}$ for each coupling field detuning Δ_c , as shown in Fig. 4(b), and accordingly reconstruct the Zak phases in Fig. 4(c), in comparison with the theoretical prediction as indicated by the dashed lines.

In conclusion, we realize the spectroscopic reconstruction of the Zak phases of superradiance lattices. Without trapping atoms or controlling their velocities [9, 11, 12], we take advantage of the atomic thermal motion [46, 47] and locate the anti-crossing points of the WSLs, which give out the values of the Zak phases. This method can be directly generalized to measure Chern numbers in two dimensional lattices [17, 31] by introducing more coupling fields [48–50] in the current framework as well as in photonic lattices [51] and synthetic dimensions [52, 53]. Our results push forward the room-temperature quantum simulation of topological phases and pave the way to detect multipole moments in higher-order topological insulators [19, 34, 35].

The authors thank Luqi Yuan for useful discussions. This work was supported by the National Key Research and Development Program of China (Grants

No. 2019YFA0308100 and No. 2018YFA0307200), the National Natural Science Foundation of China (Grants No.11934011 and No. 11874322), Zhejiang Province Key Research and Development Program (Grant No. 2020C01019), the Strategic Priority Research Program of Chinese Academy of Sciences (Grant No. XDB28000000), and the Fundamental Research Funds for the Central Universities. H.C. was supported by the China Postdoctoral Science Foundation (Grant No. 2021M692838).

*These authors contributed equally to this work.

[†]hancai@zju.edu.cn

[1] M. Z. Hasan and C. L. Kane, Colloquium: Topological insulators, *Rev. Mod. Phys.* **82**, 3045 (2010).

[2] X. L. Qi and S. C. Zhang, Topological insulators and superconductors, *Rev. Mod. Phys.* **83**, 1057 (2011).

[3] J. Zak, Berry's phase for energy bands in solids, *Phys. Rev. Lett.* **62**, 2747 (1989).

[4] K. Von Klitzing, G. Dorda, and M. Pepper, New Method for High-Accuracy Determination of the Fine-Structure Constant Based on Quantized Hall Resistance, *Phys. Rev. Lett.* **45**, 494 (1980).

[5] D. J. Thouless, M. Kohmoto, M. P. Nightingale, and M. den Nijs, Quantized Hall Conductance in a Two-Dimensional Periodic Potential, *Phys. Rev. Lett.* **49**, 405 (1982).

[6] F. D. M. Haldane, Model for a quantum Hall effect without Landau levels: condensed-matter realization of the "parity anomaly", *Phys. Rev. Lett.* **61**, 2015 (1988).

[7] D. W. Zhang, Y. Q. Zhu, Y. X. Zhao, H. Yan, and S. L. Zhu, Topological quantum matter with cold atoms, *Advances in Physics*, **67**, 253 (2018).

[8] N. R. Cooper, J. Dalibard, and I. B. Spielman, Topological bands for ultracold atoms, *Rev. Mod. Phys.* **91**, 015005 (2019).

[9] M. Atala, M. Aidelsburger, J. T. Barreiro, D. Abanin, T. Kitagawa, E. Demler, and I. Bloch, Direct measurement of the Zak phase in topological Bloch bands, *Nat. Phys.* **9**, 795 (2013).

[10] L. Duca, T. Li, M. Reitter, I. Bloch, M. Schleier-Smith, and U. Schneider, An Aharonov-Bohm interferometer for determining Bloch band topology, *Science* **347**, 288 (2015).

[11] E. J. Meier, F. A. An, A. Dauphin, M. Maffei, P. Massig-nan, T. L. Hughes, B. Gadway, Observation of the topological Anderson insulator in disordered atomic wires, *Science* **362**, 929 (2018).

[12] D. Xie, W. Gou, T. Xiao, B. Gadway, and B. Yan, Topological characterizations of an extended Su-Schrieffer-Heeger model, *npj Quantum Inf.* **5**, 1 (2019).

[13] M. Aidelsburger, M. Lohse, C. Schweizer, M. Atala, J. T. Barreiro, S. Nascimbène, N. R. Cooper, I. Bloch, and N. Goldman, Measuring the Chern number of Hofstadter bands with ultracold bosonic atoms, *Nat. Phys.* **11**, 162 (2015).

[14] T. Chalopin, T. Satoor, A. Evrard, V. Makhlov, J. Dalibard, R. Lopes, and S. Nascimbene, Probing chiral edge dynamics and bulk topology of a synthetic Hall system, *Nat. Phys.* **16**, 1017 (2020).

[15] D. N. Maksimov, E. N. Bulgakov, and A. R. Kolovsky, Wannier-Stark states in double-periodic lattices. I. One-dimensional lattices, *Phys. Rev. A* **91**, 053631 (2015).

[16] D. N. Maksimov, E. N. Bulgakov, and A. R. Kolovsky, Wannier-Stark states in double-periodic lattices. II. Two-dimensional lattices, *Phys. Rev. A* **91**, 053632 (2015).

[17] W. R. Lee and K. Park, Direct manifestation of topological order in the winding number of the Wannier-Stark ladder, *Phys. Rev. B* **92**, 195144 (2015).

[18] A. R. Kolovsky, Topological phase transitions in tilted optical lattices, *Phys. Rev. A* **98**, 013603 (2018).

[19] A. N. Poddubny, Distinguishing trivial and topological quadrupolar insulators by Wannier-Stark ladders, *Phys. Rev. B* **100**, 075418 (2019).

[20] G. H. Wannier, Dynamics of Band Electrons in Electric and Magnetic Fields, *Rev. Mod. Phys.* **34**, 645 (1962).

[21] N. Marzari, A. A. Mostofi, J. R. Yates, I. Souza, and D. Vanderbilt, Maximally localized Wannier functions: Theory and applications, *Rev. Mod. Phys.* **84**, 1419 (2012).

[22] R. D. King-Smith and D. Vanderbilt, Theory of polarization of crystalline solids, *Phys. Rev. B* **47**, 1651R (1993).

[23] R. Resta, Macroscopic polarization in crystalline dielectrics: the geometric phase approach, *Rev. Mod. Phys.* **66**, 899 (1994).

[24] S. Kivelson, Wannier functions in one-dimensional disordered systems: Application to fractionally charged solitons, *Phys. Rev. B* **26**, 4269 (1982).

[25] M. J. Rice and E. J. Mele, Elementary Excitations of a Linearly Conjugated Diatomic Polymer, *Phys. Rev. Lett.* **49**, 1455 (1982).

[26] D. W. Wang, R. B. Liu, S. Y. Zhu, and M. O. Scully, Superradiance Lattice, *Phys. Rev. Lett.* **114**, 043602 (2015).

[27] L. Chen, P. Wang, Z. Meng, L. Huang, H. Cai, D. W. Wang, S. Y. Zhu, and J. Zhang, Experimental Observation of One-Dimensional Superradiance Lattices in Ultracold Atoms, *Phys. Rev. Lett.* **120**, 193601 (2018).

[28] C. Mi, K. S. Nawaz, L. Chen, P. Wang, H. Cai, D. W. Wang, S. Y. Zhu, and J. Zhang, Time-resolved interplay between superradiant and subradiant states in superradiance lattices of Bose-Einstein condensates, *Phys. Rev. A* **104**, 043326 (2021).

[29] M. O. Scully, E. S. Fry, C. H. Ooi, and K. Wódkiewicz, Directed spontaneous emission from an extended ensemble of N atoms: Timing is everything, *Phys. Rev. Lett.* **96**, 010501 (2006).

[30] W. P. Su, J. R. Schrieffer, and A. J. Heeger, Solitons in polyacetylene, *Phys. Rev. Lett.* **42**, 1698 (1979).

[31] S. Coh and D. Vanderbilt, Electric Polarization in a Chern Insulator, *Phys. Rev. Lett.* **102**, 107603 (2009).

[32] R. Yu, X. L. Qi, A. B. Bernevig, Z. Fang, and X. Dai, Equivalent expression of Z_2 topological invariant for band insulators using the non-Abelian Berry connection, *Phys. Rev. B* **84**, 075119 (2011).

[33] M. Taherinejad, K. F. Garrity, and D. Vanderbilt, Wannier center sheets in topological insulators, *Phys. Rev. B* **89**, 115102 (2014).

[34] W. A. Benalcazar, B. A. Bernevig, and T. L. Hughes, Quantized electric multipole insulators, *Science* **357**, 61 (2017).

[35] M. Ezawa, Higher-Order Topological Insulators and

Semimetals on the Breathing Kagome and Pyrochlore Lattices, *Phys. Rev. Lett.* **120**, 026801 (2018).

[36] See Supplemental Material for experimental setup, absorption rate, effective Hamiltonian derivation, and supplementary data figures, which includes Ref. [37–39].

[37] T. Ozawa and I. Carusotto, Anomalous and Quantum Hall Effects in Lossy Photonic Lattices, *Phys. Rev. Lett.* **112**, 133902 (2014).

[38] H. Cai, J. Liu, J. Wu, Y. He, S. Y. Zhu, J. X. Zhang, and D. W. Wang, Experimental Observation of Momentum-Space Chiral Edge Currents in Room-Temperature Atoms, *Phys. Rev. Lett.* **122**, 023601 (2019).

[39] Y. He, R. Mao, H. Cai, J. X. Zhang, Y. Li, L. Yuan, S. Y. Zhu, and D. W. Wang, Flat-Band Localization in Creutz Superradiance Lattices, *Phys. Rev. Lett.* **126**, 103601 (2021).

[40] J. Wang, Y. Zhu, K. J. Jiang, and M. S. Zhan, Bichromatic electromagnetically induced transparency in cold rubidium atoms, *Phys. Rev. A* **68**, 195144 (2003).

[41] S. Yu Kruchinin, F. Krausz, and V. S. Yakovlev, Colloquium: Strong-field phenomena in periodic systems, *Rev. Mod. Phys.* **90**, 021002 (2018).

[42] S. Glutsch and F. Bechstedt, Interaction of Wannier-Stark ladders and electrical breakdown in superlattices, *Phys. Rev. B* **60**, 16584 (1999).

[43] H. Koochaki Kelardeh, V. Apalkov, and M. I. Stockman, Wannier-Stark states of graphene in strong electric field, *Phys. Rev. B* **90**, 085313 (2014).

[44] S. Kuang, R. Wan, P. Du, Y. Jiang, and J. Gao, Transmission and reflection of electromagnetically induced absorption grating in homogeneous atomic media, *Opt. Express* **16**, 15455 (2008).

[45] G. H. Wannier, Wave functions and effective Hamiltonian for Bloch electrons in an electric field, *Phys. Rev.* **117**, 432 (1960).

[46] P. Peng, W. Cao, C. Shen, W. Qu, J. Wen, L. Jiang, and Y. Xiao, Anti-parity-time symmetry with flying atoms, *Nat. Phys.* **12**, 1139 (2016).

[47] S. Zhang, Y. Hu, G. Lin, Y. Niu, K. Xia, J. Gong, and S. Gong, Thermal-motion-induced non-reciprocal quantum optical system, *Nat. Photon.* **12**, 744 (2018).

[48] Z. Zhang, F. Li, G. Malpuech, Y. Zhang, O. Bleu, S. Koniakhin, C. Li, Y. Zhang, M. Xiao, and D. D. Solnyshkov, Particlelike Behavior of Topological Defects in Linear Wave Packets in Photonic Graphene, *Phys. Rev. Lett.* **122**, 233905 (2019).

[49] J. Yuan, C. Wu, L. Wang, G. Chen, and S. Jia, Observation of diffraction pattern in two-dimensional optically induced atomic lattice, *Opt. Lett.* **44**, 4123 (2019).

[50] J. Yuan, H. Zhang, C. Wu, L. Wang, L. Xiao, and S. Jia, Tunable optical vortex array in a two-dimensional electromagnetically induced atomic lattice, *Opt. Lett.* **46**, 4184 (2021).

[51] T. Ozawa, H. M. Price, A. Amo, N. Goldman, M. Hafezi, L. Lu, M. C. Rechtsman, D. Schuster, J. Simon, O. Zilberman, and I. Carusotto, Topological photonics, *Rev. Mod. Phys.* **91**, 015006 (2019).

[52] L. Yuan, Q. Lin, M. Xiao, and S. Fan, Synthetic dimension in photonics, *Optica* **5**, 1396 (2018).

[53] A. Dutt, Q. Lin, L. Yuan, M. Minkov, M. Xiao, and S. Fan, A single photonic cavity with two independent physical synthetic dimensions, *Science* **367**, 59 (2020).